ACS APPLIED MATERIALS & INTERFACES

RESEARCH ARTICLE

www.acsami.org

Superhydrophobicity of Natural and Artificial Surfaces under Controlled Condensation Conditions

Long Yin,[†] Lin Zhu,[†] Qingjun Wang,[†] Jianfu Ding,[‡] and Qingmin Chen*[,†]

[†]Polymer Science and Engineering Department, School of Chemistry and Chemical Engineering, State Key Laboratory of Coordination Chemistry, Nanjing University, Nanjing, Jiangsu 210093, China

[‡]Institute for Chemical Process and Environmental Technology, National Research Council Canada, Ottawa, Ontario K1A0R6, Canada

ABSTRACT: In this paper, we have comparatively investigated the stability of superhydrophobic behaviors of fresh and biomimetic lotus leaf surfaces under controlled water condensation conditions. The binary micro/nano structures of the superhydrophobic surfaces are observed with electron micrographs. Contact and sliding angles are evaluated by syringing water droplets on the substrates with surface temperatures and humidity precisely controlled between −10 and 30 °C, and RH = 10, 30, 60, and 90%. According to the calculations on the solid−liquid contact area fraction in different environmental conditions based on a micro/nano binary structure model, the effects of condensed water on superhydrophobic surfaces are assessed quantitatively. Both the calculated and experimental results indicate that the temperature difference between surface temperature and the dew point during measurement is essential to the occurrence of water condensation while the effect of condensation on the surface wettability also depends on the topology of hierarchical structured surfaces. The loss of water repellency that usually appears on the artificial superhydrophobic surface under low temperature and high humidity conditions is proved to be reversible, showing a bidirectional transition of the equilibrium state between Wenzel and Cassie−Baxter.

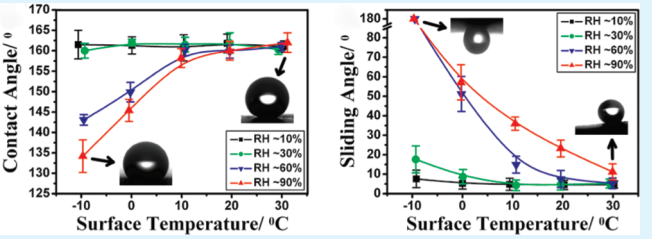

KEYWORDS: superhydrophobic, condensation, contact angle, sliding angle, surface temperature, relative humidity

INTRODUCTION

Superhydrophobic surface usually refers to a solid surface with a water contact angle larger than 150° and a sliding angle less than 10°.[1] The phenomenon of superhydrophobicity, also known as "lotus effect",[2] is common in nature, for example many plant surfaces[3] and insect wings.[4] The lotus leaf is always regarded as a symbol of purity in East Asia due to its impressive self-cleaning property, stemming from a micro/nano binary structured surface covered with a hydrophobic wax layer.[5] Inspired by the high water repellency of the lotus leaf, artificial superhydrophobic surfaces have been constructed via two primary approaches: one is to modify a hierarchical surface with low-surface-energy materials,[6−8] and the other is to roughen the surface of hydrophobic materials.[5,9,10] These surfaces have attracted much attention in recent years because of their potential applications in icephobic materials for antenna and conveyance,[11−13] drag-reduction and antifouling for marine vessels,[14−17] and self-cleaning coatings for buildings.[18,19]

The wettability of a solid surface depends mainly on a combination of the chemical composition and the surface topology.[20] Young recognized that the intrinsic contact angle of a smooth surface was closely correlated to the interfacial tensions, and proposed the famous Young's equation in 1805.[21]

$$\cos\theta = (\gamma_{sv} - \gamma_{sl})/\gamma_{lv} \quad (1)$$

where θ is the equilibrium contact angle on a smooth substrate of a homogeneous material, γ_{sv}, γ_{sl} and γ_{lv} are the solid−gas, solid−liquid and liquid−gas interfacial tensions, respectively. According to eq 1, the difference between solid−gas and solid−liquid interfacial tensions plays an important role in determining the wetting behavior for a smooth surface. When $\gamma_{sv} - \gamma_{sl} > 0$, a hydrophilic surface is determined ($\theta < 90°$), while a hydrophobic surface ($\theta > 90°$) is obtained when $\gamma_{sv} - \gamma_{sl} < 0$.

Two theoretical regimes are independently proposed by Wenzel[22] and by Cassie and Baxter[23] for a liquid droplet on topologically roughed and chemically inhomogeneous surfaces. In the Wenzel state, a water droplet can wet the entire microstructures on the surface, and the apparent contact angle of a rough surface, θ_W, is described by the following equation

$$\cos\theta_W = r\cos\theta \quad (2)$$

where r, termed the roughness factor, is defined as the ratio of the actual to projected solid−liquid contact area on the horizontal plane. In the Cassie−Baxter state, a water droplet is incapable of penetrating into valleys of the microstructures with air trapped between the droplet and the substrate, resulting in a composite surface of solid and air. The apparent

Received: January 18, 2011
Accepted: March 28, 2011
Published: March 28, 2011

contact angle, θ_{CB}, is given by

$$\cos\theta_{CB} = f(\cos\theta + 1) - 1 \quad (3)$$

where f denotes the fraction of solid−liquid contact area. The transition from the Cassie−Baxter to the Wenzel state may probably occur when the required energy barrier is overcome by a droplet.[24−26]

Recently, the effects of water condensation on the wetting behaviors of natural and artificial superhydrophobic surfaces have attracted much attention.[27−38] However, the experimental results about the stability of superhydrophobicity of the lotus leaf under dew condensation conditions are somewhat controversial. Several researchers indicated the possibility of a transition from hydrophobic to hydrophilic.[27−29] Contrarily, a constant water repellency of the lotus leaf was also reported by comparing contact and sliding angles with other plants under water condensation conditions.[30,31] For biomimic surfaces, it was concluded on basis of literatures that the wettability of microstructured surfaces was greatly increased,[32−34,37] whereas several lotus-like micro/nano hierarchical structured and nanostructured surfaces retained their superhydrophobicity well when condensation indeed occurred.[30,35,36] This research was concerned more with the relationship between the architectural characteristics of various surfaces and their superhydrophobic stability under condensation conditions. However, only a very limited number of publications have systemically investigated the effect of environmental factors on the wettability of superhydrophobic surfaces.[31,37] In one of our previous works, a facile dip-coating process was adopted to prepare a highly durable superhydrophobic surface on paint films.[7] For the present study, we will compare this surface with fresh lotus leaf to evaluate the effect of controllable condensation on the surface wettability by adjusting temperature and humidity to anticipated conditions. The transition of a water droplet between Cassie−Baxter to the Wenzel state was realized by changing dew condensation conditions.

EXPERIMENTAL SECTION

Materials. Perfluoroalkyltriethoxysilanes $[CF_3(CF_2)_nCH_2CH_2Si(OC_2H_5)_3$, PFO$]$ (n = 6−8) were purchased from Fluorochem. SiO_2 nanoparticles were obtained from Cabot. Bisphenol-A epoxy resin (E−44) and 2,5-diamino-3,6-dimethylmercaptotoluene (E−300) were obtained from Albemarle. Methanol, acetone, and hydrochloric acid (HCl, 37 wt %) were analytical regents and used without further purification. Epoxy paint and aluminum alloy plates were supplied by Polymer Engineering Material Research Center of Nanjing University and Southwest Aluminum (6061, China), respectively.

Preparation of Superhydrophobic Surfaces. The lotus leaves were cultivated in the Star Lake in Nanjing University, China. The leaf samples of 15 × 15 mm^2 were cut from similar areas and the upper sides were used for study. The commercial aluminum alloy plates in the same size were spray-coated with epoxy paint and cured at 23 °C for 24 h. The thickness of the paint film was estimated in the range of 100−200 μm. To manufacture superhydrophobic surface, we created microstructures on the paint surface by sandblasting it with brown emery (60#) under 0.8 MPa pressure condition, followed by thoroughly cleaning with deionized water in an ultrasonic bath and drying at room temperature. A SiO_2/epoxy adhesive solution was prepared by mixing a SiO_2 nanoparticle solution in acetone with an epoxy adhesive solution, which were prepared by dispersing SiO_2 nanoparticles (1.0 g) in acetone (100 mL) under ultrasonication for 1 h and mixing E−44 (1.0 g) and E−300 (0.2 g) into acetone (100 mL), respectively. The nanostructures were then introduced by dip-coating the sandblasted substrate with the SiO_2/epoxy adhesive solution for two or three times followed by curing in an oven at 60 °C for 2 h. The obtained SiO_2 anchored surface was then modified by an as-prepared PFO solution, which was prepared by dissolving 0.5 wt % PFO in a mixture of methanol (88 wt %), deionized water (10 wt %) and HCl (0.1M, 1.5 wt %), by dipping for four times and then cured at 100 °C for 5 h.

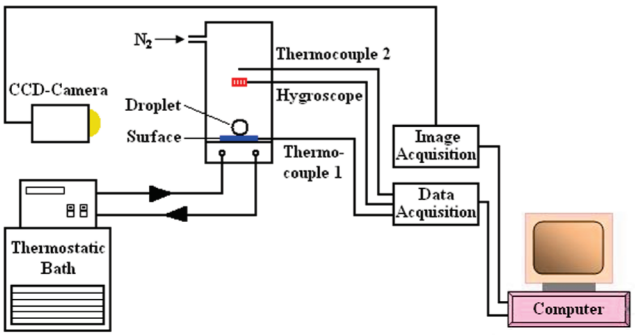

Figure 1. Schematic of the experimental device designed for contact and sliding angle measurement under controllable environmental conditions.

Instrumentation. The water contact angles (CAs) and sliding angles (SAs) were evaluated by utilizing a modified optical angle meter (Cam 200, KSV Instrument Ltd., Finland). The experimental setup was schematically shown in Figure 1.[12,39,40] The sample stage was assembled in a homemade environment chamber for obtaining a stable microclimate with controlled humidity and temperature. The environmental control system consisted of a thermostatic bath, two ultrasensitive T-type thermocouples (WRCK-Φ1.0 mm, Changzhou Puruite Temperature Wire Factory, China), a nitrogen/water vapor flux, a hygroscope and a data acquisition system (Personal Daq/3000, IO tech. Inc., USA). The thermostatic bath could precisely maintain the surface temperature (T_{surf}) of superhydrophobic samples from −30 to 40 °C by mean of a heated/refrigerated circulator, and the thermocouples were used to record surface and air temperatures simultaneously. The relative humidity (RH) inside the chamber was regulated by adjusting the feeding rate of dry nitrogen and water vapor, and measured by a hygroscope with a relative error of about 3%. All data transmission to the computer was carried out through the data acquisition system. A highspeed CCD-camera and an image acquisition system were applied to take real-time photographs and to transfer droplet images to the computer for further analysis of the static and dynamic behaviors of water droplets at the contact line. The CAs were tested by syringing deionized water to superhydrophobic surfaces according to the sessile drop method. The chamber was mounted on a rotatable platform, which was driven by a DC step electric motor to tilt the sample stage at a fixed angular velocity of 0.1°/s. The SAs were obtained when water droplets began to slide down the inclined test surface. Water droplets of 5 or 10 μL were acquired for the measurement of CAs or SAs, respectively. The reported results were the average of 10 measured values.

The morphology of the superhydrophobic specimens was investigated by a field-emission scanning electron microscopy (SEM, Hitachi S−4800, Japan). All samples for SEM imaging were sputtered with a thin layer of gold (2 nm) before observation.

RESULTS AND DISCUSSION

The surface topographies of the lotus leaf and the as-prepared artificial superhydrophobic sample were studied by SEM with the images shown in Figure 2. Figure 2a−c clearly displays binary

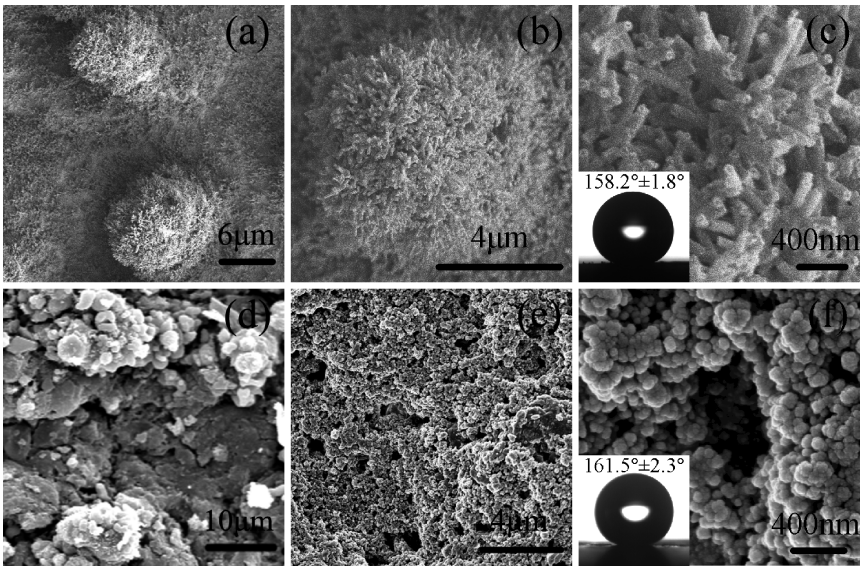

Figure 2. SEM images at magnifications of (a) 2000×, (b) 10000×, and (c) 40000× of the lotus leaf and at magnifications of (d) 1500×, (e) 5000×, and (f) 40000× of artificial superhydrophobic surface. The insets refer to water contact angles measured on each substrate.

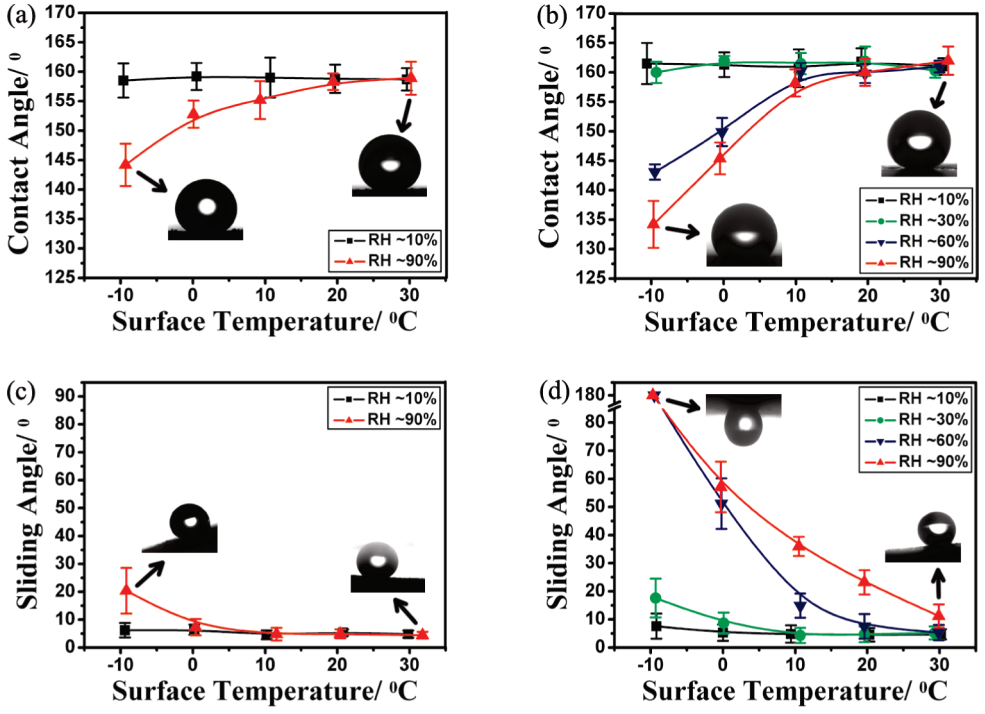

Figure 3. Water CAs and SAs on (a, c) the lotus leaf and (b, d) the artificial superhydrophobic surface from −10 to 30 °C under different RH. The insets represent images of water droplets during measurement.

structures of the fresh lotus leaf, which consist of microprotuberances with diameters ranging from 5−20 μm and numerous nanotubes of 100−150 nm vertically assembled all over the surface, which was covered a wax layer. Recent experiments reported that the wax on the lotus leaf surface was weakly hydrophilic and the static contact angle of the smooth wax surface is about 74°.[27,41] The artificial superhydrophobic surface was stepwise prepared. A microstructured surface decorated with protrusions of about 10 μm was fabricated by sandblasting the paint film, as shown in Figure 2d. Anchoring SiO_2 nanoparticles at sizes of 50−100 nm on the sandblasted surface led to micro/nano hierarchical structures, which were shown in Figure 2e (low magnification) and Figure 2f (high magnification). Then this micro/nano hierarchical surface was treated with a PFO solution to form the artificial superhydrophobic surface. The contact angle of the smooth PFO coating surface is 105.0° ± 2.0°.

Figure 3 compares water CAs and SAs on the lotus leaf and the artificial superhydrophobic surface at different T_{surf} and RH. As many works have been done on the superhydrophobicity of the lotus leaf,[27−31] in this work, only extremely low and high RHs of

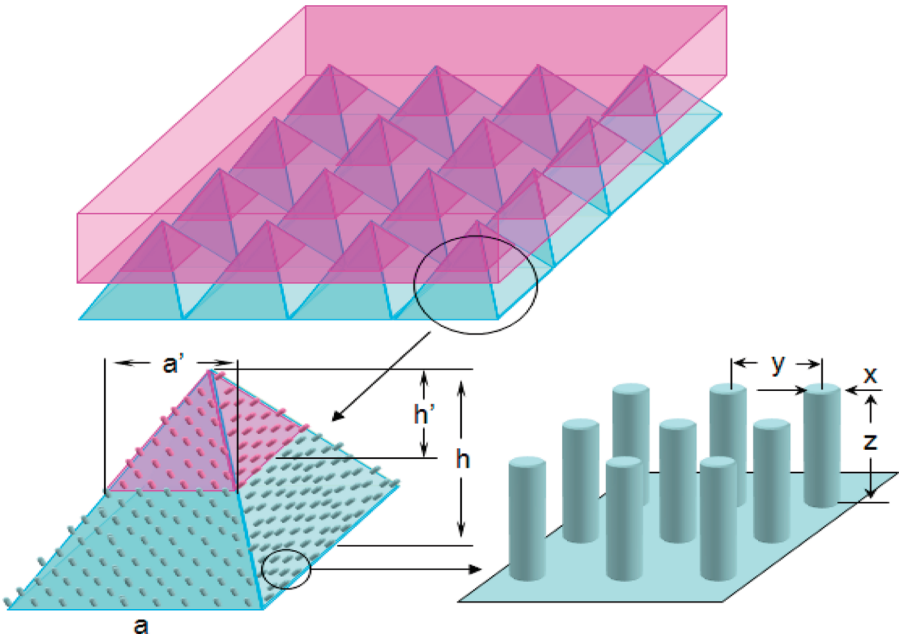

Figure 4. Micro/nano binary model integrated a pyramid array with a cylinder array for describing the topological structure and wetting process of the lotus leaf, where *a* and *h* are the spacing and height of the microprotuberances, and *x*, *y*, and *z* are the diameter, spacing and height of the nanotubes anchored on the surface. A water droplet (red layer) is suspended on the pyramid array with the tip at a height of *h*′ wetted (red area).

10% and 90% were tested for the lotus leaf, while CAs and SAs of the artificial superhydrophobic surface were tested under four RHs of 10%, 30%, 60% and 90%. Previous research has shown that water will become supercooled without freezing when the temperature falls below 0 °C under the conditions similar to this work.[12] Figure 3 shows that there is CAs of both surfaces do not have temperature dependence under a low RH of 10%. The CAs keep constant with average values of 158.8° ± 2.6° and 161.3° ± 2.5° between −10 and 30 °C on natural (Figure 3a) and artificial (Figure 3b) samples, respectively. The maintenance of the high water repellency is mainly attributed to two factors: micro/nano structures[31] and extremely low humidity. Under such a low RH, the dew point temperature (T_d) is far below T_{surf}. T_d is defined as the temperature at which water vapor in the air reaches saturation and some must condense into liquid water at constant barometric pressure. As a result, water condensation does not occur on surfaces even when the T_{surf} was −10 °C at this humidity. Furthermore, similar results are observed under RH of 30%. However, it is shown that the CAs decrease significantly as the T_{surf} declines below 10 °C when RH climbs above 60%. Under a high RH of 90%, the CAs become 152.8° ± 2.3° at 0 °C and 144.2° ± 3.6° at −10 °C on the lotus leaf, and correspondingly 145.4° ± 2.7° and 134.2° ± 4.0° on the artificial surface.

Although the contact angle of a surface is commonly used as a criterion to assess the hydrophobicity, it is insufficient to evaluate the water repellent property of superhydrophobic surfaces.[42,43] For self-cleaning, the movement of water droplets at low inclination angles is required. Therefore, the sliding angle (SA), defined as the inclination angle where a droplet begins to slide off a surface, is also measured in the same conditions. As shown in Figure 3c, the averaged SAs on lotus leaf change little and fluctuate at 4−6° under RH of 10%. In response to the decreased CAs under RH of 90%, the SAs rise to 20.2 ± 8.2° when the T_{surf} declines to −10 °C. As the SA is closely correlated to contact angle hysteresis,[44] the increase of SAs reflects enhanced interaction between water and solid. Although the artificial superhydrophobic surface has outstanding water repellency with the SAs of about 5° under RH of 10%, the SAs show a slow increase with the decreased T_{surf} under RH of 30%, finally reaching 17.6 ± 6.9° at −10 °C (Figure 3d). Under RH of 60% or 90%, the surface adhesion of the artificial sample increases much faster than that of the lotus leaf at low temperatures (T_{surf} < 10 °C). Additionally, it is worthwhile to note that water droplets are strongly adhered to the cold substrate at −10 °C and can no longer roll away even overturning the surface. Consequently, it is confirmed that the water repellent property is completely lost under this extremely low temperature and high humidity condition.

The CAs measured under RH lower than 30% on both surfaces are coincident with the apparent CAs of the Cassie−Baxter state. In this condition, a water droplet shaped as a sphere is "suspended" on a composite surface, and the air pocket between water and the substrate plays an important role in reducing the solid−liquid interaction. However, the average contact angle of the lotus leaf reduces to 144.2° at −10 °C and RH of 90%, therefore the water droplet should be partially in the Cassie−Baxter state. Zheng et al.[29] have in situ investigated water condensation on the lotus leaf at micro- and nanoscales and observed that the binary structures remained intact under RH of about 70%, whereas a thin layer of water was formed on tops of protuberances with some water penetrated into the interspaces among nanotubes under RH of about 100%. This dew condensation under a high humidity might partially convert the surface from Cassie−Baxter state to Wenzel state. Furthermore, the CAs of the artificial superhydrophobic surface at −10 °C and RH of 90% are much lower (134.2° ± 4.0°). It means more preexisted air replaced by condensed water, indicating a much easier conversion from Cassie−Baxter state to Wenzel state of this surface.

For easy understanding the correlation of surface topological structure with the wetting behavior, a micro/nano binary model is proposed to describe the topological structure of the lotus leaf in Figure 4, where a and h are the spacing and height of the pyramid array, representing the microprotuberances, and x, y and z are the diameter, spacing and height of the cylinder array, representing the nanotubes anchored on the surface. When a water droplet is placed on the surface, because of the superhydrophobic property of the lotus leaf, the water droplet was suspended on the pyramid array. Only the tip of the pyramid with a height of h' contacts with water to form the solid−liquid contact area (red area), whereas the rest was the air−liquid contact area (green area). The wetting behavior of the whole surface should follow Cassie−Baxter equation[45]

$$\cos\theta^* = f\cos\theta' + (1-f)\cos 180^\circ \quad (4)$$

where θ^* is the apparent contact angle, and f is the solid−liquid contact area fraction, according to the model in Figure 4, $f = (a'/a)^2 = (h'/h)^2$. θ' is the contact angle of the solid−liquid contact area. The first part of the right side of eq 4 represents the contribution from the solid−liquid contact area, where one possible condition is that water can penetrate into the space between the nanotubes. Under this condition, the wetting behavior of this solid−liquid contact area follows Wenzel model,[22] and then eq 4 can be rewritten as

$$\cos\theta^* = rf\cos\theta + (f-1) \text{ or } f = (\cos\theta^* + 1)/(r\cos\theta + 1) \quad (5)$$

where θ is the equilibrium contact angle of the smooth surface of the same material, r is roughness factor defined as the ratio of the actual to projected solid−liquid contact area on the horizontal plane. It should be noted the same equation was also derived by other groups using post,[46,47] pore,[47] and needle[38,43] models. The r value can be calculated from the structure parameters, a, h, x, y, and z of the model as defined in Figure 4 using the following equation.

$$r = [1 + (2h/a)^2]^{1/2}[\pi xz + y^2]/y^2 \quad (6)$$

The other condition in this solid−liquid contact area is that water only partially contacts with the substrate, as described by Cassie−Baxter mode. This condition might more commonly existed, especially at a low humidity and a high temperature. Under this condition, if one treated the "wet" part and the "dry" part in this solid−liquid contact area as wholes, the effect of this area to the wetting behavior of the whole surface will be equivalent to a surface at the first condition, but with a small solid−liquid contact area, i.e., following eq 5 with a smaller f value. Therefore, eq 5 can also be used for treating this condition. Under this situation, the calculated f value will be smaller than its real value.

As a result, eq 5 will be used in the following discussion for the all experiments conducted under the different conditions in this work. It should be bore in mind that the calculated results are equivalent to the first condition, where water in the solid−liquid contact area completely wetted the surface. For the calculation, the parameters in eq 6 can be estimated from the SEM images of the lotus leaf and the results are: $a = 22\,\mu$m, $h = 16\,\mu$m, $x = 85$ nm, $y = 300$ nm, $z = 600$ nm. Therefore, the r value of the lotus leaf can be calculated to be 4.91. The r value of the artificial superhydrophobic surface was also estimated by using the same model

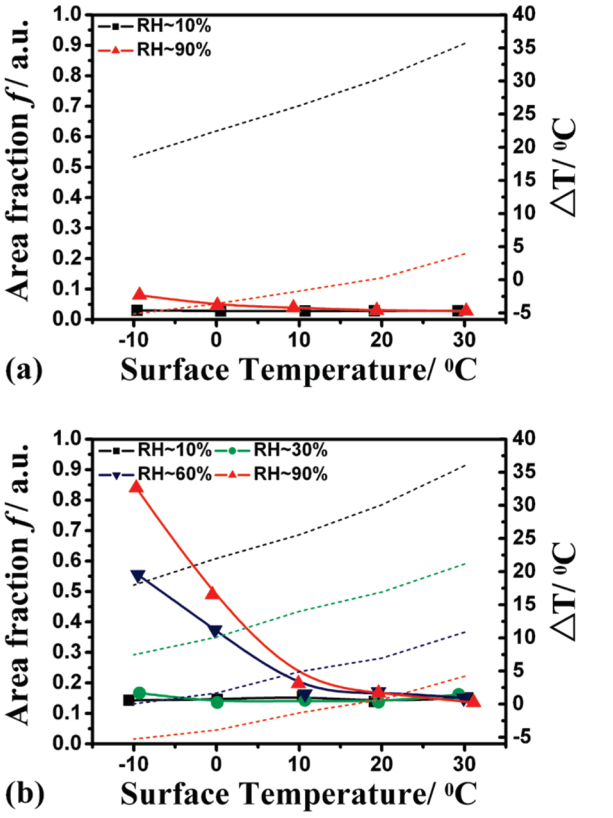

Figure 5. The change of the solid−liquid contact area fraction (f, solid line) and temperature difference (ΔT, dashed line) of (a) the lotus leaf and (b) the artificial superhydrophobic surface by varying T_{surf} and RH.

to approximately represent the topological structure with the parameters estimated from the SEM images being: $a = 40\,\mu$m, $h = 20\,\mu$m, $x = 30$ nm, $y = 50$ nm, and $z = 20$ nm. The produced r values are 2.47. Inputting this r value and the equilibrium contact angle ($\theta = 74^\circ$ and 105°, respectively for lotus leaf and the artificial superhydropobic surface) into eq 4, the solid liquid fraction of the both surfaces under different humidity and temperature can be calculated from the apparent contact angle (θ^*). Therefore, panels a and b in Figure 3 were replotted in Figure 5 in the term of f varied with temperature under the humidity of RH = 10, 30, 60, and 90%.

Figure 5 shows the f of the lotus leaf is always low with the values smaller than 0.1, even under a very high humidity and a low temperature (RH = 90%, $T_{surf} = -10$ °C), though under this condition the CAs reduce dramatically from 159° to 144°. However, the f value of the artificial superhydrophobic surface remains relatively high, larger than 0.1. Furthermore, under a high humidity (RH = 60% or 90%), this value promptly increases with the decrease of temperature and reaches almost unity under RH = 90% and $T_{surf} = -10$ °C, meaning the surface is nearly completely wetted by water. This might explain the extremely high sliding angle under this condition. A careful comparison of Figure 3c and 3d with Figure 5a and 5b respectively reveals a same trend of the sliding angle and the f value changed with temperature for the individual surface, indicating a high level correlation between the sliding angle and the f value. It is easy to understand that the higher f value means higher fraction of the solid−liquid contact area, resulting in a higher interaction between solid and liquid. It will apparently increase the resistance

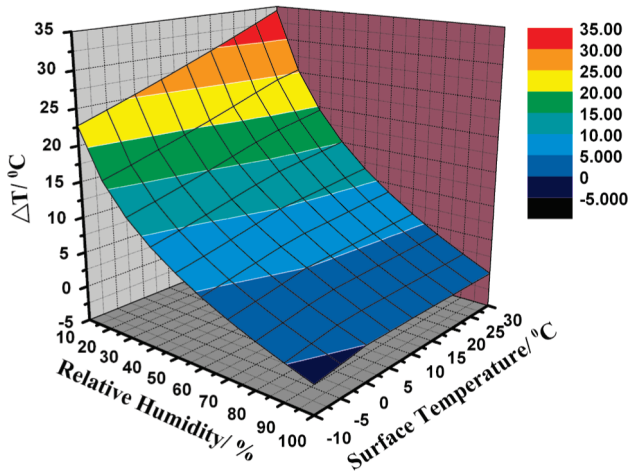

Figure 6. Temperature difference (ΔT) as a function of the surface temperature and air relative humidity.

for a water droplet sliding on the surface. This result also indicates that a low solid−liquid area fraction is essential for obtaining a surface with a low sliding angle.

In order to better understand the results in Figure 5, ΔT at different surface temperatures was also plotted in the Figure 5. It is defined as the difference between the surface temperature and the calculated dew point temperature by the following equation:

$$\Delta T = T_{surf} - T_d \quad (7)$$

where T_{surf} is the surface temperature in situ acquired by Thermocouple 1, and T_d is the dew point temperature calculated based on the relative humidity (Hygroscope) used in the experiment according to literature.[48] It shows that the f of the lotus leaf remains lower than 0.03 under RH of 10%, meanwhile ΔT is very large, no matter what the T_{surf} is. Even at −10 °C, the ΔT is still larger than 18 °C. In the absence of necessary conditions for water condensation, the lotus leaf retains its superhydrophobicity well throughout. Under RH of 90%, the ΔT falls to −1.7 at 10 °C and continues to decline when the T_{surf} continues to decrease. It means that water becomes able to condense on the leaf surface, leading to slowly increased fractions of the solid−liquid contact area from 0.028 to 0.080 when the T_{surf} changes from 30 to −10 °C. On the other hand, although similar behavior was demonstrated under a low humidity with RH of 10% and 30%, it is found that the artificial superhydrophobic surface is more susceptible to water condensation than the lotus leaf (Figure 5b). The f values at −10 °C imply that the liquid−air fraction decreased quickly and about 49% and 84% of the solid substrate directly contacts with water under RH of 60 and 90%, respectively. This significant difference of the wetting behavior between the two surfaces, induced by water condensation under high dew condensation conditions with low T_{surf} and high RH, is apparently correlated with the differences of both the contact angle of the surface material and the topological structures of the two surfaces as indicated by eq 4. The lotus leaf surface is integrated with numerous tube-like nanostructures with diameters of 100−150 nm, which grow upward on the microprotuberances and the base of valleys. As a result, on the basis of the prediction of the Wenzel equation, the high surface roughness can restrict water to only wet a small area on the top of the microprotuberances, leading to a very small value of f. This result agrees with the observation in another work, where it is observed that the tops of microprotuberances become more wettable under water condensation to create a wettability gradient that moves condensed microdroplets along the exterior surface of the protuberance directionally from the valley to the top. This effect results in nearly all the condensed microdroplets being suspended on the tops rather than the valleys of protuberances.[29] However, the roughness of the artificial superhydrophobic surface is much lower (r = 2.47 vs 4.91 for lotus leaf predicted by the binary model employed in Figure 4). Water can easily condense in the spaces between the protrusions, causing a prompt increase of the solid−liquid contact area under high RH.

Table 1. Contact and Sliding Angle (deg) for the Superhydrophobic Surfaces under Condensation and Restoration Condition

	contact angle		sliding angle	
	condensation	restoration	condensation	restoration
lotus leaf	144.2 ± 3.6	158.5 ± 2.5	20.4 ± 8.2	4.0 ± 1.1
artificial Surface	134.2 ± 4.0	160.9 ± 2.2		4.2 ± 1.9

Inspired by the connection of the ΔT with the f, we look forward to the general principle of the influence of environmental factors on the surface wettability. The ΔT is proved to be a vital factor to decide whether water vapor in atmosphere condenses into liquid on superhydrophobic surfaces, so the relationship with varied surface temperature and relative humidity is calculated, as shown in Figure 6. It is demonstrated that the ΔT is always larger than 5 °C under RH lower than 60%, and therefore water condensation hardly occurs in this condition. When the decrease of T_{surf} is accompanied with the increase of the RH, the ΔT gradually reaches 0 °C, meaning a promoted possibility of condensation on cold substrates. It is noteworthy that in the deep blue region where the T_{surf} is below 0 °C and RH is above 90%, condensation appears an inevitable phenomenon because the substrate is colder than the condensate temperature of water. This is in accordance with the experimental results that the wettability of the two superhydrophobic surfaces is more or less affected by low T_{surf} and high RH.

An experiment about the wettability restoration of two superhydrophobic surfaces is carried out to identify whether the loss of superhydrophobicity triggered by water condensation is reversible. The tested samples at −10 °C and RH of 90% are laid in Petri dishes under an ambient condition for 24 h, and the CAs and SAs are immediately remeasured under RH of 30%. The data in Table 1 show that although water condensation causes a temporary loss of water repellency, the superhydrophobic behaviors of both surfaces are well resumed after evaporation of condensed water. This observation is consistent with reported results on porous nanostructured carbon films.[49] After a drying process in air, the sliding behavior of water droplets was observed again because of removal of water from the pores.

CONCLUSION

The aim of this work is to evaluate the effect of environmental factors on the wettability of superhydrophobic surfaces under controlled condensation conditions. The artificial superhydrophobic surface has been fabricated by a facile dip-coating process. We have developed an experimental system to accurately control temperature and humidity for contact and sliding angle

measurements. It is indicated that superhydrophobic behaviors of both natural and artificial surfaces are unaffected under a low RH (<60%). Under a high RH (>60%), when the surface temperature is getting closer to the dew point temperature, an increased wettability characterized by decreasing contact angles and increasing sliding angles is observed on the two surfaces due to the incremental amount of condensed water. Therefore, it is important to provide the experimental condition including temperature and humidity when water contact and sliding angles are reported. In spite of that, the lotus leaf shows a much better repellent property to water condensation because of its unique hierarchical structures. Water is easier to condense among microstructures of the artificial superhydrophobic surface, and the decrease of the contact angle suggests a transition of the equilibrium from Cassie−Baxter to Wenzel state. Fortunately, the loss of superhydrophobicity is restorable when condensed water vanishes. The results help us to understand the synergetic effects of the structure and environment on water repellency. The ingenious construction and fine environmental adaptability are desired for superhydrophobic surfaces to get more applications in industry, such as the self-cleaning in rain and anti-icing in winter.

AUTHOR INFORMATION

Corresponding Author

*Tel.: 86-25-83593289. Fax: 86-25-83593048. Email: chenqm@nju.edu.cn.

ACKNOWLEDGMENT

The authors thank Ms. Zhou for technical assistance with SEM measurement. This work is financially supported by a grant Nanjing University Testing Fund (0205D100).

REFERENCES

(1) Sun, T. L.; Feng, L.; Gao, X. F.; Jiang, L. *Acc. Chem. Res.* **2005**, *38*, 644–652.
(2) Barthlott, W.; Neinhuis, C. *Planta* **1997**, *202*, 1–8.
(3) Neinhuis, C.; Barthlott, W. *Ann. Bot.* **1997**, *79*, 667–677.
(4) Wagner, T.; Neinhuis, C.; Barthlott, W. *Acta Zool.* **1996**, *77*, 213–225.
(5) Feng, L.; Li, S.; Li, Y.; Li, H.; Zhang, L.; Zhai, J.; Song, Y.; Liu, B.; Jiang, L.; Zhu, D. *Adv. Mater.* **2002**, *14*, 1857–1860.
(6) Sarkar, D. K.; Farzaneh, M.; Paynter, R. W. *Mater. Lett.* **2008**, *62*, 1226–1229.
(7) Cui, Z.; Yin, L.; Wang, Q. J.; Ding, J. F.; Chen, Q. M. *J. Colloid Interface Sci.* **2009**, *337*, 531–537.
(8) Xu, X. H.; Zhang, Z. Z.; Yang, J. *Langmuir* **2010**, *26*, 3654–3658.
(9) Erbil, H. Y.; Demirel, A. L.; Avci, Y.; Mert, O. *Science* **2003**, *299*, 1377–1380.
(10) Shiu, J. Y.; Kuo, C. W.; Chen, P. L.; Mou, C. Y. *Chem. Mater.* **2004**, *16*, 561–564.
(11) Cao, L. L.; Jones, A. K.; Sikka, V. K.; Wu, J. Z.; Gao, D. *Langmuir* **2009**, *25*, 12444–12448.
(12) Yin, L.; Xia, Q.; Xue, J.; Yang, S. Q.; Wang, Q. J.; Chen, Q. M. *Appl. Surf. Sci.* **2010**, *256*, 6764–6769.
(13) Meuler, A. J.; Smith, J. D.; Varanasi, K. K.; Mabry, J. M.; McKinley, G. H.; Cohen, R. E. *ACS Appl. Mater. Interfaces* **2010**, *2*, 3100–3110.
(14) Shirtcliffe, N. J.; McHale, G.; Newton, M. I.; Zhang, Y. *ACS Appl. Mater. Interfaces* **2009**, *1*, 1316–1323.
(15) Yali, Z.; Mei, L.; Bin, S.; Qinghua, L. *J. Mater. Chem.* **2009**, *19*, 3301–3306.
(16) Genzer, J.; Efimenko, K. *Biofouling* **2006**, *22*, 339–360.
(17) Scardino, A. J.; Zhang, H.; Cookson, D. J.; Lamb, R. N.; de Nys, R. *Biofouling* **2009**, *25*, 757–767.
(18) Zhang, X. T.; Sato, O.; Taguchi, M.; Einaga, Y.; Murakami, T.; Fujishima, A. *Chem. Mater.* **2005**, *17*, 696–700.
(19) Niu, J. J.; Wang, J. N. *J. Phys. Chem. B* **2009**, *113*, 2909–2912.
(20) Chou, T. H.; Hong, S. J.; Sheng, Y. J.; Tsao, H. K. *J. Phys. Chem. B* **2010**, *114*, 7509–7515.
(21) Young, T. *Philos. Trans. R. Soc. Lond.* **1805**, *95*, 65–87.
(22) Wenzel, R. N. *Ind. Eng. Chem.* **1936**, *28*, 988–994.
(23) Cassie, A. B. D. *Discuss. Faraday Soc.* **1948**, *3*, 11–16.
(24) Lafuma, A.; Quere, D. *Nat. Mater.* **2003**, *2*, 457–460.
(25) Patankar, N. A. *Langmuir* **2004**, *20*, 7097–7102.
(26) Dupuis, A.; Yeomans, J. M. *Langmuir* **2005**, *21*, 2624–2629.
(27) Cheng, Y. T.; Rodak, D. E. *Appl. Phys. Lett.* **2005**, *86*, 144101−1–3.
(28) Cheng, Y. T.; Rodak, D. E.; Angelopoulos, A.; Gacek, T. *Appl. Phys. Lett.* **2005**, *87*, 194112−1–3.
(29) Zheng, Y. M.; Han, D.; Zhai, J.; Jiang, L. *Appl. Phys. Lett.* **2008**, *92*, 084106−1–3.
(30) Mockenhaupt, B.; Ensikat, H. J.; Spaeth, M.; Barthlott, W. *Langmuir* **2008**, *24*, 13591–13597.
(31) Yin, L.; Wang, Q. J.; Xue, J.; Ding, J. F.; Chen, Q. M. *Chem. Lett.* **2010**, *39*, 816–817.
(32) Narhe, R. D.; Beysens, D. A. *Phys. Rev. Lett.* **2004**, *93*, 076103–1−4.
(33) Wier, K. A.; McCarthy, T. J. *Langmuir* **2006**, *22*, 2433–2436.
(34) Jung, Y. C.; Bhushan, B. *J. Microsc.* **2008**, *229*, 127–140.
(35) Chen, C. H.; Cai, Q. J.; Tsai, C. L.; Chen, C. L.; Xiong, G. Y.; Yu, Y.; Ren, Z. F. *Appl. Phys. Lett.* **2007**, *90*, 173108–1−3.
(36) Dorrer, C.; Ruhe, J. *Adv. Mater.* **2008**, *20*, 159–163.
(37) Karmouch, R.; Ross, G. G. *J. Phys. Chem. C* **2010**, *114*, 4063–4066.
(38) Furuta, T.; Sakai, M.; Isobe, T.; Nakajima, A. *Langmuir* **2010**, *26*, 13305–13309.
(39) Wang, Q. J.; Yin, L.; Yang, S. Q.; He, D.; Chen, Q. M. *Chinese Patent Application 200910034767.5*, 2009.
(40) Wang, Q. J.; Yin, L.; Xue, J.; Chen, Q. M. *Chinese Patent Application 200910034768.X*, 2009
(41) Cheng, Y. T.; Rodak, D. E.; Wong, C. A.; Hayden, C. A. *Nanotechnology* **2006**, *17*, 1359–1362.
(42) Murase, H.; Fujibayashi, T. *Prog. Org. Coat.* **1997**, *31*, 97–104.
(43) Miwa, M.; Nakajima, A.; Fujishima, A.; Hashimoto, K.; Watanabe, T. *Langmuir* **2000**, *16*, 5754–5760.
(44) Furmidge, C. G. L. *J. Colloid Sci.* **1962**, *17*, 309–324.
(45) Marmur, A. *Langmuir* **2003**, *19*, 8343–8348.
(46) Werner, O.; Wagberg, L.; Lindstrom, T. *Langmuir* **2005**, *21*, 12235–12243.
(47) Jopp, J.; Grull, H.; Yerushalmi-Rozen, R. *Langmuir* **2004**, *20*, 10015–10019.
(48) Lawrence, M. G. *J. Am. Meteorol. Soc.* **2005**, *86*, 225–233.
(49) Xiao, X. C.; Cheng, Y. T.; Sheldon, B. W.; Rankin, J. *J. Mater. Res.* **2008**, *23*, 2174–2178.